On the Feasibility of Using the Intrinsic Fluorescence of Nucleotides for DNA Sequencing

ARTICLE *in* THE JOURNAL OF PHYSICAL CHEMISTRY C · APRIL 2010

Impact Factor: 4.77 · DOI: 10.1021/jp911229c · Source: PubMed

On the Feasibility of Using the Intrinsic Fluorescence of Nucleotides for DNA Sequencing†

Mustafa H. Chowdhury,‡ Krishanu Ray,‡ Michael L. Johnson,§ Stephen K. Gray,|| James Pond,⊥ and Joseph R. Lakowicz*,‡

Center for Fluorescence Spectroscopy, Department of Biochemistry and Molecular Biology, University of Maryland School of Medicine, 725 West Lombard Street, Baltimore, Maryland 21201, Departments of Pharmacology and Internal Medicine, University of Virginia Health System, Box 800735, Charlottesville, Virginia 22908, Center for Nanoscale Materials, Argonne National Laboratory, Argonne, Illinois 60439, and Lumerical Solutions Inc., 201−1290 Homer Street, Vancouver, British Columbia, Canada V6B 2Y5

Received: November 25, 2009; Revised Manuscript Received: February 12, 2010

There is presently a worldwide effort to increase the speed and decrease the cost of DNA sequencing as exemplified by the goal of the National Human Genome Research Institute (NHGRI) to sequence a human genome for under $1000. Several high throughput technologies are under development. Among these, single strand sequencing using exonuclease appear very promising. However, this approach requires complete labeling of at least two bases at a time, with extrinsic high quantum yield probes. This is necessary because nucleotides absorb in the deep ultraviolet (UV) and emit with extremely low quantum yields. Hence intrinsic emission from DNA and nucleotides is not being exploited for DNA sequencing. In the present paper we consider the possibility of identifying single nucleotides using their intrinsic emission. We used the finite-difference time-domain (FDTD) method to calculate the effects of aluminum nanoparticles on nearby fluorophores that emit in the UV. We find that the radiated power of UV fluorophores is significantly increased when they are in close proximity to aluminum nanostructures. We show that there will be increased localized excitation near aluminum particles at wavelengths used to excite intrinsic nucleotide emission. Using FDTD simulation we show that a typical DNA base when coupled to appropriate aluminum nanostructures leads to highly directional emission. Additionally we present experimental results showing that a thin film of nucleotides show enhanced emission when in close proximity to aluminum nanostructures. Finally we provide Monte Carlo simulations that predict high levels of base calling accuracy for an assumed number of photons that is derived from the emission spectra of the intrinsic fluorescence of the bases. Our results suggest that single nucleotides can be detected and identified using aluminum nanostructures that enhance their intrinsic emission. This capability would be valuable for the ongoing efforts toward the $1000 genome.

1. Introduction

Fluorescence detection has been a valuable tool in the biosciences for over 40 years.[1−4] Most applications of fluorescence use extrinsic probes which display high extinction coefficients and quantum yields. Additionally, the intrinsic fluorescence from tryptophan is often used to study the properties of proteins. However, in contrast to proteins, the intrinsic fluorescence from nucleic acids and nucleotides is very weak. As a result DNA sequencing and genetic analysis relies almost exclusively on the use of extrinsic fluorophores which are used to label the DNA bases. Until recently it was necessary to accept and work with the spectral properties of a given fluorophore. However, during the past several years we have shown that the quantum yields of fluorophores can be increased by nonchemical through-space interactions with metallic surfaces and particles.[4−8] More recently we have shown that this effect can be extended to ultraviolet (UV) wavelengths.[9−11] Based on these studies we believe it is now possible to use metal nanoparticles to increase the quantum yields of DNA bases and to enable single strand DNA sequencing using intrinsic base fluorescence.

Our study of metal-enhanced fluorescence (MEF) of the unlabeled DNA nucleotides is motivated by the growing need for high-throughput low-cost sequencing for applications in genomics, epidemiology, diagnostics, and therapeutics. This need has been recognized by the National Human Genome Research Institute (NHGRI) which has established the goal of sequencing an entire genome for $1000.[12] There are numerous approaches to DNA sequencing which have been the subject of several reviews.[12−17] It is fair to say that fluorescence played a central role in the successful sequencing of the human genome.[17,18] Until now the vast majority of sequencing has been performed using some variant of the Sanger method,[19] which is based on the use of chain terminating dideoxy-nucleotide triphosphates (ddNTPs). These methods rely on the use of extrinsic fluorescent probes which are covalently attached to the DNA by either a labeled primer or a labeled ddNTP, followed by capillary electrophoresis (CEL).[20−22] However, the Sanger technology is too costly, time-consuming, and labor intensive to meet the demand for ultrafast and low cost sequencing that is the goal of the NHGRI $1000 genome sequencing project.[12] The major driving factor behind this endeavor is the impact that it can potentially have on human health through the sequencing of "personal genomes" as a component of individualized health care, as it can shed light

† Part of the "Martin Moskovits Festschrift".
* Corresponding author. E-mail: lakowicz@cfs.biomet.umaryland.edu.
‡ University of Maryland School of Medicine.
§ University of Virginia Health System.
|| Argonne National Laboratory.
⊥ Lumerical Solutions Inc.

10.1021/jp911229c
Published on Web 03/04/2010

on clinical diagnostics and prognostics for both common and rare inherited conditions, risk assessment and prevention. One such example is how ultra fast and ultra low cost sequencing can help the field of cancer biology. The ability to sequence and compare complete genomes from many normal, neoplastic, and malignant cells from multiple individuals will allow us to comprehensively catalogue the molecular pathways and checkpoints that undergo mutation in cancer.[13] This kind of comprehensive approach can help to fully decipher the combinations of mutations that together give rise to cancer, and in doing so can facilitate a deeper understanding of the cellular functions that are perturbed during tumorigenesis.[13] One limitation of presently used sequencing methods is the need for amplification of the DNA strands either by cloning or emulsion polymerase chain reactions (PCR). To avoid the use of PCR, there are ongoing efforts to extend the sequencing techniques to single DNA strands. Some of these methods are based on fluorescence, but a number of other methods are also being explored. These novel and/or nonoptical detection methods typically rely on the use of nanopores with electrical or other physical means of identifying the bases. In this respect, the α-hemolysin channel has demonstrated the necessary properties of continuous nongating conductance and a pore size (1.5 nm) that can ensure sequential, single-file translocation of polynucleotides.[23] The α-hemolysin based DNA sequencing technology has had several significant breakthroughs in recent times and is now also on the process of being commercialized.[24,25] However, optical detection methods are still of high interest due to their sensitivity, simplicity and robustness. Recently, advances in single-molecule DNA sequencing techniques using commercially available sequencers such as the Heliscope Single Molecule Sequencer and also nanophotonic structures such as aluminum zero-mode waveguides have enabled the development of low-cost, high speed, large read length single molecule DNA sequencing techniques that can allow the analysis of human genomic information without the need for cloning, amplification, or ligation.[26,27]

The goal of this study is to lay the groundwork for the eventual development of a fluorescence technology which would allow DNA sequencing without the use of extrinsic fluorophores. It seems likely that future sequencing technology will rely on the use of nanoholes and exonuclease or some other free running enzyme (Figure 1). This technology would provide the sequence of a single strand based on the sequential release of nucleotides by an exonuclease. This approach is being pursued by a number of laboratories and is considered to be a promising revolutionary approach to meet the goals of the $1000 genome project.[12,28−30] However, to the best of our knowledge, all of these efforts depend on the use of extrinsic fluorophores or nonoptical detection. On the basis of our experience with metal-enhanced fluorescence (MEF), we believe it is possible to design and build metallic nanostructures which will allow single strand sequencing based on exonuclease digestion by detecting and identifying nucleotides based on their intrinsic fluorescence. Our idea involves taking advantage of the ongoing efforts to develop high-throughout sequencing based on nanoholes and exonuclease catalyzed release of nucleotides. We believe it will be possible to develop metallic nanostructures which enhance the intrinsic emission from the bases and provide spectral resolution to identify single nucleotides from their intrinsic emission. However fabrication of nanoholes on aluminum films by techniques such as focused ion beam (FIB) milling leads to nanohole (nanochannels) that are not atomically flat along the edges in the axis of milling. These nanoholes will have surface roughness

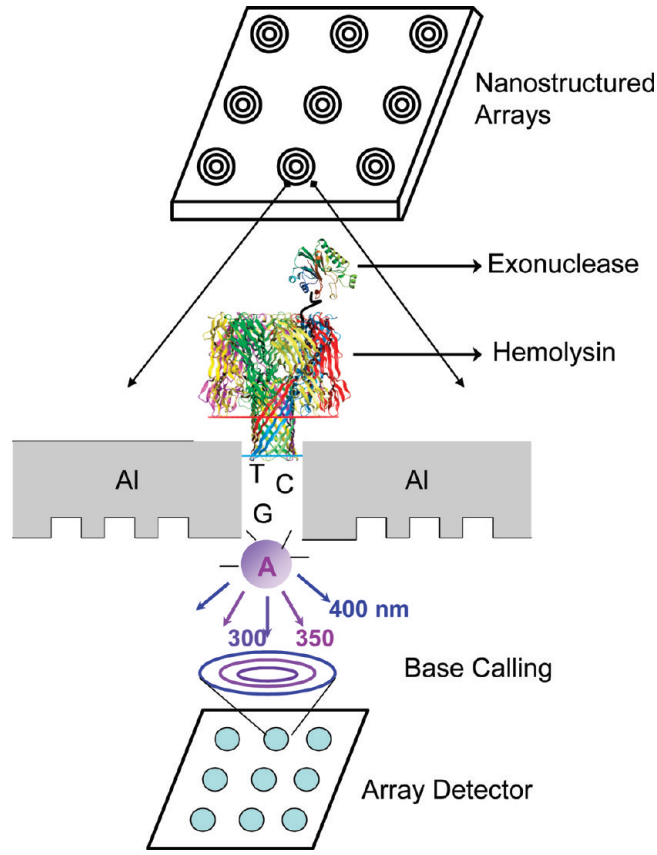

Figure 1. Schematic of our proposed nanopore based DNA sequencing system. This is based on aluminum nanostructured surfaces that can enhance both the intensity of intrinsic DNA base emission as well as increase its collection efficiency.

on the nanometer scale that can be exploited in metal-enhanced fluorescence (MEF) applications to enhance the emission intensity of the cleaved nucleotides as they pass through the channels. Additionally it might also be possible to introduce aluminum nanoparticles within the nanochannels for this specific purpose. Hence there is a need to study how aluminum particles of various sizes in the 'nm' regime can induce enhancements in the intrinsic nucleotide emission.

In this paper, we use finite-difference time domain (FDTD) calculations to explore the possibility of enhancing the intrinsic fluorescence of DNA bases with aluminum nanoparticles of various sizes and configurations.[10,31−40] The FDTD method is a rigorous computational electrodynamics method that can accurately describe plasmonic effects. We have previously used this approach to study the emission of excited-state fluorophores near one silver or aluminum nanoparticle (monomer) and between two silver nanoparticles or aluminum nanoparticles (dimer).[10,31,32] We now use the FDTD calculations to show that aluminum nanoparticles are very promising substrates for enhancing the emission of fluorophores in the spectral range relevant for DNA bases (in the UV). We show both electromagnetic near-field distributions around the aluminum nanoparticles and radiative power calculations. We also present experimental results where we show that three different nucleotides cytidine monophosphate (CMP), tyrosine monophosphate (TMP), and guanine monophosphate (GMP), when spin-coated separately on a thin particulate aluminum film on quartz substrates, show significant increases in fluorescence intensity when compared to a control quartz substrate. These experimental results corroborate our claims that aluminum nanoparticles or nanostructures can potentially be used for enhancing the intrinsic

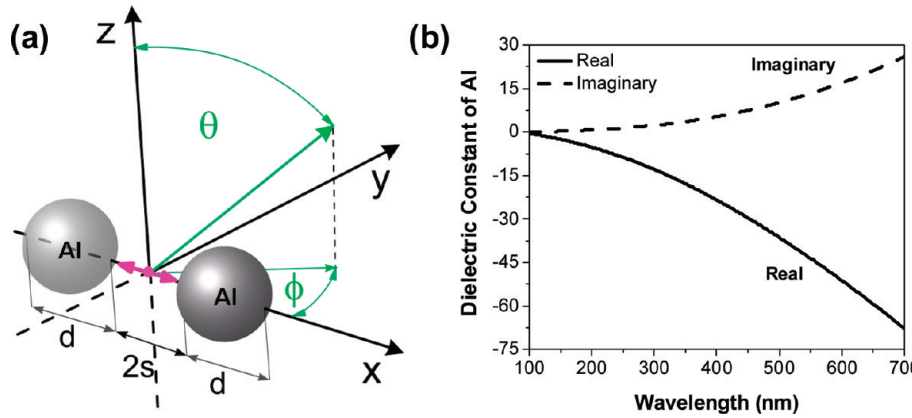

Figure 2. (a) Schematic diagram of a metal nanoparticle dimer/fluorophore system used in the FDTD calculations. The pink arrow represents the fluorophore. The fluorophores will be oriented along the x axis. The single particle (monomer) systems are identical but have one of the metal nanoparticles removed. (b) Plot of the wavelength dependent dielectric constants of aluminum used in the FDTD calculations.

emission from DNA bases. In addition to enhanced fluorescence it is thought that certain metallic geometries can result in highly directional emission. We present simulations that show a fluorophore emitting at a typical DNA base emission peak wavelength when coupled to a corrugated nanostructure containing a central nanohole on a thin aluminum film can lead to increased emission intensities and highly highly directional emission when compared to an isolated fluorophore. These calculations suggest that such nanostructures can potentially be used in nanopore based DNA sequencing experiments to both increase the emission intensity of the base emission and also significantly improve the collection efficiency of the emission. Additionally, we recognized that even with optimized nanostructures only a limited number of photons may be detectable from a single unlabeled nucleotide. Hence we performed Monte Carlo simulations that predict high levels of base calling accuracy for an assumed number of photons that is derived from the emission spectra of the intrinsic fluorescence of the bases.[41−43]

We would like to emphasize that the goal of this study is only to investigate the possibility of using aluminum nanostructures for enhancing intrinsic base fluorescence, increasing its collection efficiency, and identifying the nucleotides. It is not a blueprint of a design for an intrinsic nucleotide fluorescence based DNA sequencing system. We believe if the plasmonic properties of aluminum nanostructures can be successfully harnessed to enhance the emission intensity and also to increase the collection efficiency of emission of the low quantum yield DNA nucleotides, it might be possible in the future to potentially design low-cost high-throughput DNA sequencing systems based on intrinsic DNA base fluorescence.

2. Materials and Methods

2.1. FDTD Computational Details. Three-dimensional FDTD simulations are performed using the *FDTD Solutions* package from Lumerical Solutions, Inc. (Vancouver, Canada).[10,31,32,40] The FDTD code was implemented in the parallel option on a Dell Precision PWS690 Workstation with the following components: Dual Quad-Core Intel Xeon E5320 processors at 1.86 GHz, and 8 GB RAM. Additional postprocessing of the FDTD data were performed using *MATLAB* (version 7.0) from Mathworks (Natick, MA), and OriginPro 7 from Originlab Corporation (Northampton, MA). For calculations involving fluorophores, it is assumed that excitation of the fluorohore has already occurred and the fluorophore is now emitting dipole radiation. Hence the fluorophore is modeled as a time-windowed, oscillating point dipole source for the electric field, with frequency content spanning the spectral range (100−700 nm) of interest and polarization perpendicular to the metal nanoparticle surface. After testing for convergence, we employed a grid size of 0.5 nm for all our calculations. The typical durations of our simulations were 400 fs.

The FDTD calculations were done for a fluorophore near one aluminum nanoparticle (monomer) or between two aluminum nanoparticles (dimer). Figure 2a is a schematic illustration of the two metal nanoparticles (dimer system) where d is the diameter of each nanoparticle, $2s$ is the distance between the metal surfaces, θ is the polar angle from the z-axis where $0 \leq \theta \leq \pi$, and Φ is the azimuthal angle in the $x-y$ plane from the x axis with $0 \leq \Phi < 2\pi$. The fluorophore is placed at the origin so that it is a distance s from each metal surface. The monomer calculations correspond to simply removing one of the nanoparticles in Figure 2a. In our calculations, dipole polarizations along the x axis are considered, where the x orientation of the dipole is perpendicular to the metal nanoparticle surface. We used 1.7689 for the relative dielectric constant of water (i.e., refractive index $n = 1.33$ which is related to the dielectric constant ϵ via $\epsilon = n^2$), which is consistent with the wavelengths of light considered. In actual experiments buffered solutions will be used which typically have ion concentrations in the range of approximately 100 mM (0.1 molar) which is not enough to significantly alter the dielectric constant of water in the wavelengths of light considered in this study (100−700 nm). The FDTD program implements a realistic frequency-dependent, lossy dielectric model for aluminum.[33,40] We calculate the total radiated power enhancement as P_{rad}/P_0, where P_{rad} is the integral of the Poynting vector over a surface enclosing the fluorophore and metal nanoparticle(s), and P_0 is the result of this integral with only the fluorophore present.[10,31,32,39] This enhancement can be equated with inferences on radiative decay rate changes according to $\gamma_{rad}/\gamma^0_{rad}$, where γ_{rad} is the radiative decay rate of the dipole in proximity of the metal nanoparticle(s) and γ^0_{rad} is the radiative decay rate of an isolated dipole (in water)[39]

$$\frac{\gamma_{rad}}{\gamma^0_{rad}} = \frac{P_{rad}}{P_0} \tag{1}$$

Equation 1 implies that an enhancement in the total radiated power is indicative of a corresponding increase in the relative radiative decay rate of the system and vice versa. An increase

in the radiative rate will usually result in an increased quantum yield, unless the nonradiative processes overwhelm this effort. The optical constants of aluminum used for the FDTD calculations are presented in Figure 2b.

2.2. Experimental Details. Aluminum slugs, silicon monoxide, guanosine 3′,5′-cyclic monophaosphate sodium salt (GMP), thymidine 5′-monophosphate disodium salt hydrate (TMP), cytidine 5′-monophosphate (CMP), and low molecular weight polyvinyl alcohol (PVA, MW 13 000−23 000) were purchased from Sigma-Aldrich and used as received. Distilled water (with a resistivity of 18.2 MΩ-cm) purified using Millipore Milli-Q gradient system was used for sample preparation. Ten nm thick aluminum films were deposited on quartz slides using an Edwards Auto 306 Vacuum Evaporation chamber under high vacuum ($<5 \times 10^{-7}$ Torr). In each case, the metal deposition step was followed by the deposition of 5 nm of silica via evaporation without breaking vacuum. This step served to protect the metal surface as well as it adds a spacer layer between the metal surface and DNA bases. The deposition rate was adjusted by the filament current and the thickness of film was measured with a quartz crystal microbalance. We have reported in detail the surface roughness of the thermally evaporated aluminum films of various thicknesses in one of our previous publications.[9] Scanning electron microscope (SEM) images of films with low aluminum thickness (<20 nm) show a highly particulate surface where individual aluminum nanparticles can be clearly discerned. As the film thickness is increased it was shown that the individual particle size gradually became larger. As the aluminum film exceeded 40 nm in thickness, the metal nanoparticles coalesce to form more and more continuous surfaces which we define as a "planar surface".[9] We have reported that the 10 nm aluminum film thickness gave us the maximum MEF effect and hence we chose this thickness for our intrinsic nucleotide fluorescence studies.[9] An aliquot of approximately 500 μL of 0.5 wt % aqueous solution of low molecular weight PVA containing separately dissolved GMP, CMP and TMP was spin coated at 3000 rpm (Specialty coating system Inc., Speedline Technologies, Indiana) on the surface of the aluminum and quartz substrates respectively. This composition of PVA forms ~15 nm thick film. We verified the thickness of the spin-coated PVA films using a technique that has been reported previously.[44] The concentration of the bases in the PVA solution (before spin-coating) was approximately 1 mM. Seady-state fluorescence spectra of the DNA bases on solid substrates were recorded using a Varian Cary Eclipse Fluorescence Spectrophotometer using front face illumination.

2.3. Monte Carlo Simulations. Monte Carlo methods are simulation methods that rely on repeated random sampling to compute their results and hence can be computationally intensive.[41−43] They are useful for modeling phenomena with significant uncertainty in inputs and are especially useful in studying systems with a large number of coupled degrees of freedom, such as fluids, disordered materials, strongly coupled solids, and even complex biological systems.[41−43] In our application, Monte Carlo simulations were used to evaluate our ability to detect specific DNA bases by fluorescence techniques utilizing specific combinations of excitation and emission wavelengths. The first step is to simulate a large number (e.g., 10 000) of sets of experimental data where the correct answers are known a priori because the data was simulated. These are, of course, required to mimic the specific experimental system being evaluated, including realistic amounts of simulated measurement errors. For the present case the measurement uncertainties follow a Poisson distribution with a variance equal to the observed number of photons. The second step is to employ the proposed analysis method to analyze each of these simulated data sets to obtain "observed" results for each of the simulated data sets. The operating characteristics of the combined simulated experimental and analysis methods can then be evaluated from a comparison of the "observed results" and the correct answers that are known a priori from the simulations.

For these simulations the total number of photons is the data photons plus dark current photons summed over all of the particular excitation and emission wavelengths. The first step then is to evaluate the "expected" or "known" spectrum for each of the DNA bases at each combination excitation wavelengths, emission wavelengths, dark current and total number of photons based upon the experimentally measured spectrum of the DNA bases (Figure 8). Each of these "expected" spectra is scaled by the total number of data photons. Next, a very large number (e.g., approximately 10 000 for each of the DNA bases) of unknown data spectra are simulated from these expected spectra by adding the desired dark current and then adding measurement uncertainties corresponding to Poission distributed pseudorandom values with a variance equal to the expected spectra plus the dark current at each pair of excitation and emission wavelength.

Next, each of the "unknown" or "experimental" spectra is analyzed by weighted least-squares fitting them to four straight line functions on the "known" spectra and the known dark current, as in

$$\text{unknown}_j = \text{dark current} + \text{B}(\text{expected}_i) \qquad (2)$$

where the j subscript refers to each particular unknown spectra and the i subscript refers to each of the DNA bases. The square root of the number of photons at each excitation and emission wavelength pair is used as the weighting factors for the fitting operation. An apparent DNA base type is assigned to each of the j unknown spectra by whichever expected DNA spectra provides the lowest weighted variance-of-fit. For each of the simulated unknown spectra the correct answer is known a priori since they are actually simulated cases. The performance characteristics for each combination of total number of photons, dark current photons, and group of excitation and emission wavelengths can subsequently be evaluated by comparing the apparent DNA bases with the correct DNA bases.

3. Results and Discussion

The ability to detect and identify single unlabeled nucleotides will depend on the number of detected photons. We calculated the relative increase in signal which can be expected for a nucleotide near aluminum nanoparticles. As discussed above this increase can be found from the power radiated by a nearby dipole. These FDTD computations were performed by calculating the total radiated power as inferred by integrating the flux normal to the six sides of a closed box containing the fluorophore-nanoparticle system, and then dividing it by the corresponding power radiated by an isolated fluorophore (in water). An enhancement or quenching in the total radiated power by a system is related to relative changes in the radiative decay rate of the system in comparison to an isolated dipole as described by eq 1.[10,32,39] In our discussion, a system is defined as the excited state fluorophore−aluminum complex. Two different fluorophore−metal surface distances, $s = 2$ and 5 nm, are considered and in all cases the dipole is oriented along the x axis which is perpendicular to the surface

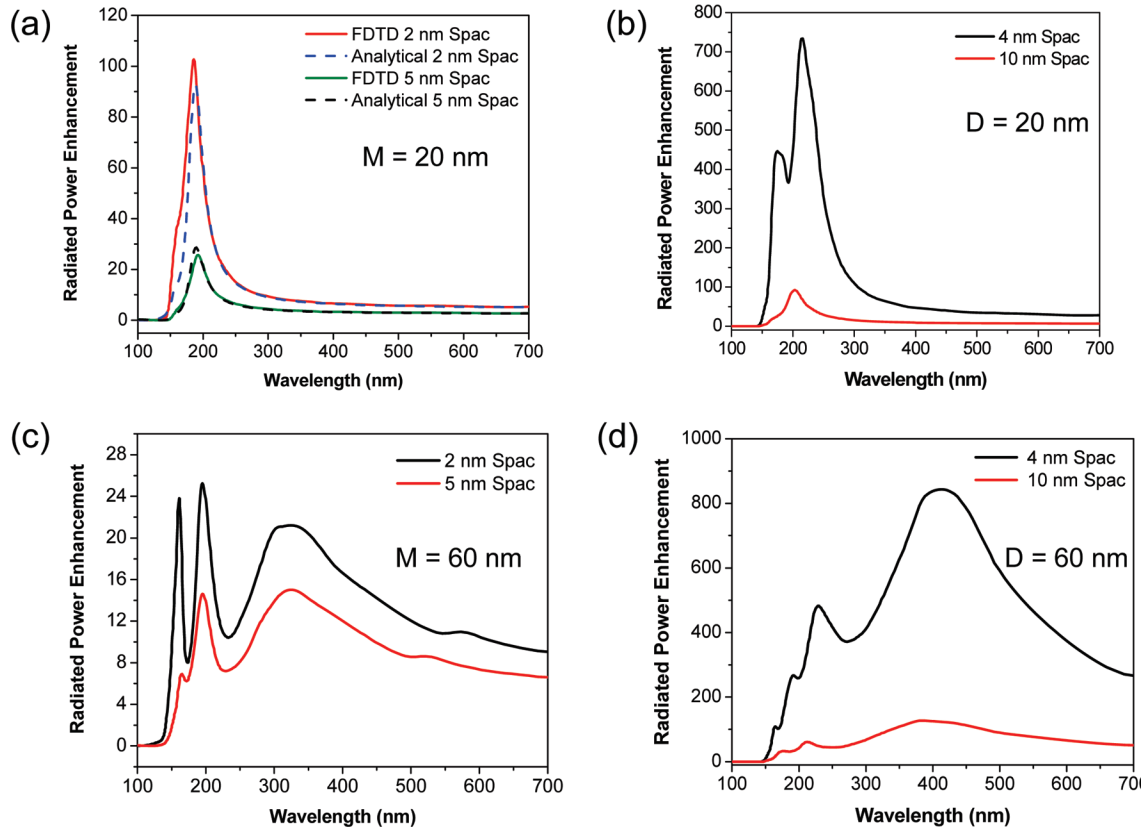

Figure 3. (a) Radiative power enhancement calculations of a fluorophore in proximity to a $d = 20$ nm aluminum nanoparticle in water (monomer = M) performed using FDTD (solid curves) and analytical theory (dashed curves). Two metal-fluorophore distances of $s = 2$ and 5 nm were studied; (b) FDTD calculations showing the radiative power enhancement of a fluorophore in the middle of a $d = 20$ nm aluminum nanoparticle dimer (D) in water. Two dimer spacings of $2s = 4$ and 10 nm were studied. The fluorophore is located exactly midway along the dimer axis. (c) FDTD calculations showing the radiative power enhancement of a fluorophore in proximity to a $d = 60$ nm aluminum nanoparticle in water (monomer = M). (d) FDTD calculations showing the radiative power enhancement of a fluorophore in the middle of a $d = 60$ nm aluminum nanoparticle dimer (D) in water.

of the metal. Figure 3a (solid curves) shows the radiated power enhancements when a fluorophore (oscillating dipole) is placed near a $d = 20$ nm aluminum nanoparticle (monomer = M) in water. We see that the enhancement in the radiated power peaks at approximately 186 nm for $s = 2$ nm separation, and at 193 nm for the $s = 5$ nm separation. It is interesting to see that the wavelength of maximum power enhancement changes with the degree of dipole−metal separation. The enhancement can be expected as in this dipole orientation, the fluorophore's dipole induces a dipole in the aluminum nanoparticle in a configuration that allows the dipoles to align along the x-axis head to tail, leading to a much larger effective radiating dipole than in the case of an isolated fluorophore (constructive interference). Given the very low quantum yields of the intrinsic emission of nucleotides compared to tryptophan or other biological chromophores, we wanted to present the "best case" scenario with the FDTD calculations. Hence we deliberately chose the x-axis orientation of the dipoles in our calculations which is perpendicular to the metal surface. We have previously shown that for fluorophores oriented parallel to the metal surface, significant quenching of the emission is observed and in cases of large metal−fluorophore distances only very modest enhancements can be seen.[10,32] We recognize that considering a complete ensemble of molecular orientations (both parallel and perpendicular) would provide more "realistic" predictions for enhancement, but we chose to present the "best case" scenario for reasons discussed above. We also observe that the degree of radiated power enhancement is dependent on the fluorophore-metal distance with $s = 2$ nm showing significantly more enhancement than the $s = 5$ nm case. It is also encouraging to note that $d = 20$ nm aluminum nanoparticles give excellent enhancements (approximately 100-fold) at short metal−dipole distances ($s = 2$ nm) and the enhancements at longer distances ($s = 5$ nm) is quite significant as well (approximately 25-fold).

An exact analytical solution, based on Mie theory, can be developed for the case of a radiating point dipole and a single metal sphere.[45] Figure 3a also shows as dashed curves the exact analytical results, which agree very well with the numerical FDTD results. This agreement gives us confidence that our results involving two metal spheres, for which no analytical solution is available, are valid.

It is known from the plasmonics literature that greatly enhanced fields are induced by light incident on particle dimers. It is also known that fluorescence can be enhanced more for fluorophores between particles than near a single particle.[10,32] Figure 3b shows the radiated power enhancements when a fluorophore (radiating dipole) is placed exactly midway between an aluminum dimer system where each nanoparticle has a diameter of $d = 20$ nm. Here two dimer separation distances of $2s = 4$ and 10 nm were chosen. Essentially these systems are the dimer analogues of the monomers studied in Figure 3a. We see that the presence of dimers significantly increases the amount of enhancement observed. For the $2s = 4$ nm, we see maximum enhancements of over 700-fold at approximately 215 nm. For the $2s = 10$ nm case, we see maximum enhancements of over 90-fold at

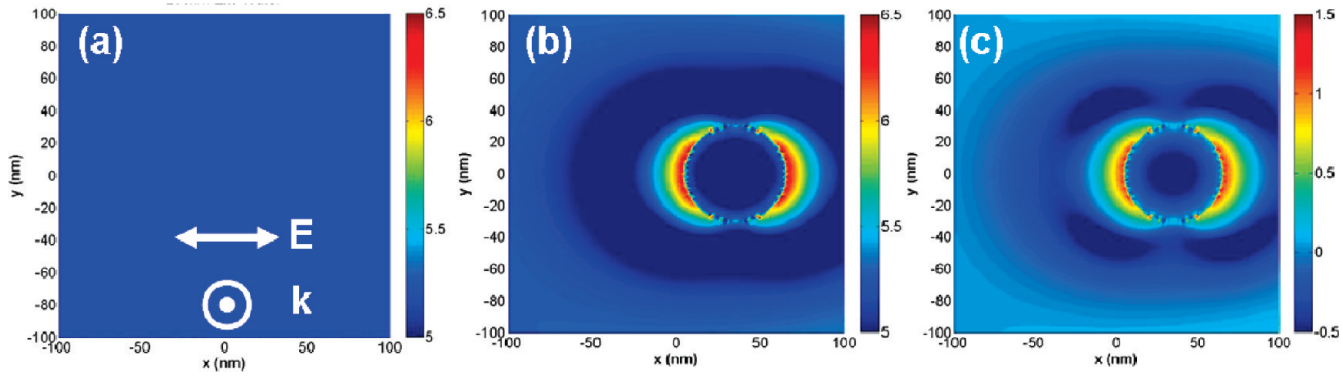

Figure 4. (a) Near-field intensity image in water of a plane wave of wavelength 260 nm oriented along the x axis and propagating along the z axis (out of the plane of paper). (b) Near-field intensity image of the fields created around a $d = 60$ nm aluminum nanoparticle by its interaction with the plane wave of panel a. (c) Near-field image of the field enhancement around a $d = 60$ nm Al nanoparticle by its interaction with the plane wave of panel a. This image is generated by diving the data of panel b by that of panel a. Note all images are in the log scale (base 10).

approximately 203 nm. It is interesting to observe again that the wavelength of maximum enhancement shift with changes in dipole−metal distance. For both the separation distances in the dimer case (specially for the $2s = 4$ nm case), we observe a shoulder in the wavelength dependent radiative power enhancement spectra that is blue-shifted with regard to the main peak. The large enhancements in the case of the dimers occurs because the fluorophore's dipole induces two dipoles of the same polarity, one in each of the aluminum nanoparticles in the dimer system. This configuration allows all the three dipoles to align along the x-axis head-to-tail, leading to a much larger effective radiating dipole than in case of the isolated dipole or a single nanoparticle−fluorophore system.

Figure 3c shows the radiated power enhancements when a fluorophore is placed near a $d = 60$ nm aluminum nanoparticle. Like the case of the $d = 20$ nm nanoparticles, we studied two dipole-metal distances of $s = 2$ and 5 nm. Here we see strong radiative power enhancements as a function of wavelength with the maximum enhancement of approximately 21-fold at 321 nm for the $s = 2$ nm case, and we also observe secondary enhancement peaks of approximately 25-fold at 196 nm, and 24-fold at 162 nm. For the $s = 5$ nm case, we observe an approximately 15-fold enhancement at 321 nm, and additional secondary enhancement peaks of approximately 14-fold at 196 nm and 6-fold at 162 nm. These results show that the wavelength of peak radiative power enhancement red-shifts with an increase in particle size. This is similar to our earlier reported observations.[10] In Figure 3d, we obtain the radiative power enhancement for the dipole in between two $d = 60$ nm aluminum nanoparticles in a dimer system. Here we see a significant increase in the radiative power enhancement, with a primary peak enhancement of approximately 860-fold at 410 nm for the $2s = 4$ nm case. We also observe additional secondary enhancement peaks of approximately 480-fold at 230 nm and 260-fold at 190 nm, respectively. For the $2s = 10$ nm case, we observe a peak enhancement of approximately 137-fold at 387 nm. We also observe additional secondary enhancement peaks of approximately 65-fold at 213 nm and 37-fold at 170 nm, respectively. We believe these secondary peaks are due to higher order enhancement modes and become more prominent as the fluorophore comes in closer proximity to the metal, an observation we have reported earlier.[10] An important overall conclusion from these calculations is that significant enhancements are expected for a wide range of particle sizes, clusters, and distances. Additionally the enhancements are expected over a wide range of wavelengths, especially from 300 to 400 nm where the nucleotides emit. Hence we expect aluminum nanostructures to be generally useful in enhancing intrinsic DNA emission.

Single molecule detection of visible wavelength fluorophores is usually accomplished using confocal optics to minimize the observed volume around the fluorophore. This is necessary to decrease the unavoidable background emission and scattering which can overwhelm the emission from a single fluorophore. This problem is expected to become greater at the UV wavelengths needed to excite nucleotide emission. Metal particles can be used to decrease the effective observed volume by localization of the fields near the surface of the particles. Additionally, the near-field information can provide insight into the nature of metal enhanced fluorescence that is interesting from the perspective of applications involving molecular spectroscopy and designing specific fluorophore-metal nanoparticle systems. Figure 4 shows and discusses the effect of 260 nm plane wave excitation on the near-fields around a $d = 60$ nm aluminum nanoparticle in water. A wavelength of 260 nm was chosen for our calculations because it is typical for the excitation of DNA nucleotide fluorescence. All the near-field calculations shown are performed along a single plane, that is, the $x-y$ plane running through the center of the aluminum nanoparticles. In Figure 4a, we show the near-field intensity image ($E^2 = E_x^2 + E_y^2 + E_z^2$) in water of a plane wave of wavelength 260 nm with its electric field oriented along the x axis and its propagation vector along the z axis (out of the plane of paper). Since we are observing the plane wave along its planar wavefront, we see an image of uniform intensity. Figure 4b shows the near-fields intensities around a $d = 60$ nm aluminum nanoparticle created by its interaction with the plane wave of Figure 4a. Figure 4c shows the image of the near-field enhancements around the $d = 60$ nm aluminum nanoparticle by its interaction with the plane wave of Figure 4a. This image is generated by dividing the raw data of Figure 4b by the data of Figure 4a. Note all images are in the log scale (base 10). Figure 4c clearly reveals that the interaction of aluminum nanoparticles with 260 nm incident light produces regions of high field enhancements around the nanoparticle. The field intensity patterns in these regions show an enhancement of over 10-fold in some areas. It is interesting to note that the field intensity is somewhat decreased at distances ranging from 20 to 50 nm from the aluminum nanoparticle. This is an interesting effect which may contribute to small effective excited volumes near metal particles.

Figure 5a−c shows respectively the electric field intensity in the $x-y$ plane ($E^2 = E_x^2 + E_y^2 + E_z^2$) of a plane wave of

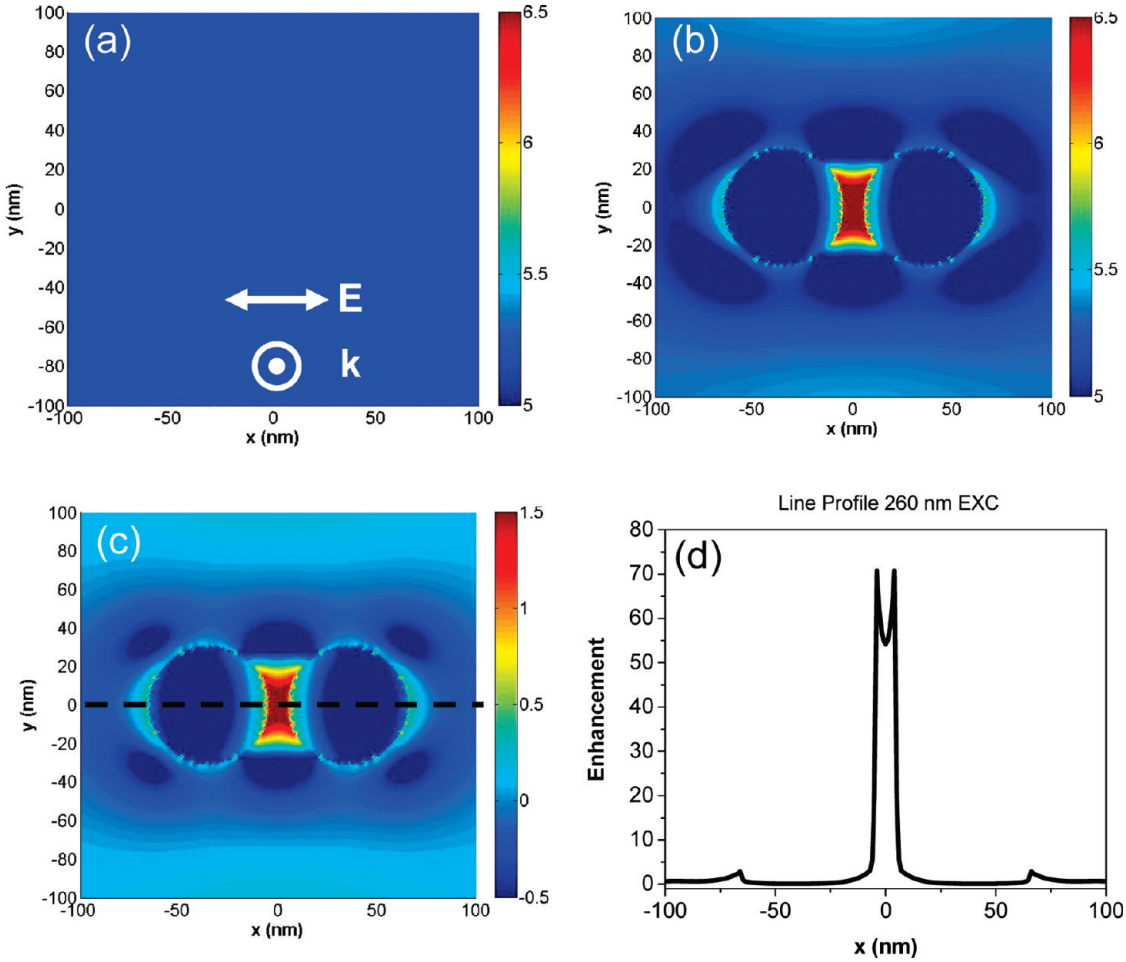

Figure 5. (a) Near-field intensity image in water of a plane wave of wavelength 260 nm oriented along the x axis and propagating along the z axis (out of the plane of paper). (b) Near-field intensity image of the fields created around a $d = 60$ nm aluminum nanoparticle dimer spaced $2s = 10$ nm by its interaction with the plane wave of panel a. (c) Near-field image of the field enhancement around a $d = 60$ nm aluminum nanoparticle dimer by its interaction with the plane wave of panel a. This image is generated by dividing the raw data of panel b by that of panel a. Note all images are in the log scale (base 10). (d) A line profile taken from the central part of the enhancement image showing maximum enhancements of approximately 70-fold in between the dimers.

wavelength 260 nm, the near-fields around a $d = 60$ nm aluminum nanoparticle dimer system with a surface-to-surface distance of $2s = 10$ nm, and the near-field enhancement and quenching image that was calculated by dividing the raw data of Figure 5b by the data of Figure 5a. Figure 5d shows a line profile taken from the central part of the enhancement image [Figure 5c] showing maximum enhancements of approximately 70-fold in between the dimers. These areas of high near-field enhancements in between the particles means that a DNA base molecule (or any other fluorophore) once localized between the dimers will experience a much higher excitation field than if it were isolated and directly excited only by the incident light. This will lead to higher excitation rates of the fluorophore, which leads to greater excitation−emission cycles in a given time period. It is interesting to note that the high field enhancements localized in a small region between the particles may also contribute to smaller effective excitation volumes near the particles. Additionally, the relative contribution of unwanted background noise from the sample will be decreased because of the lower relative excitation field intensities outside of the central region. The enhanced radiation power calculations presented in Figure 3 signifies an increase in the radiative decay rate of the fluorophore-metal system (when the fluorophore is in proximity to the aluminum particle). This increase in the radiative decay rate can also potentially decrease the excited state lifetime of the fluorophore. Thus a shorter excited-state lifetime combined with an increased excitation−emission cycle can translate to an increase in the number of photons emitted by the fluorophore in a given time period (providing the excited-state molecule is not saturated). This set of FDTD calculations suggest that a dimer or a cluster of aluminum nanoparticles can significantly enhance the intensity of the emission of any nucleotides that are in proximity to it.

In the previous paragraph, we considered the fields induced by the incident light. We now consider the fields induced by an excited state nucleotide near an aluminum nanoparticle. We believe this is important because it is the system of dipole plus particle that radiates to the far-field and increased induced near-fields most probably indicates increased far-field radiation. Figure 6 presents the effect of an excited-state fluorophore emitting at 350 nm on the near-fields around a $d = 60$ nm aluminum nanoparticle. We choose 350 nm as this wavelength is in emission region of the intrinsic fluorescence of DNA bases. We kept the fluorophore or dipole oscillating at a fixed frequency corresponding to 350 nm throughout the entire simulation time, and constructed a time average of the square of the electric field vector over the last period of evolution. The calculations in Figure 6 show

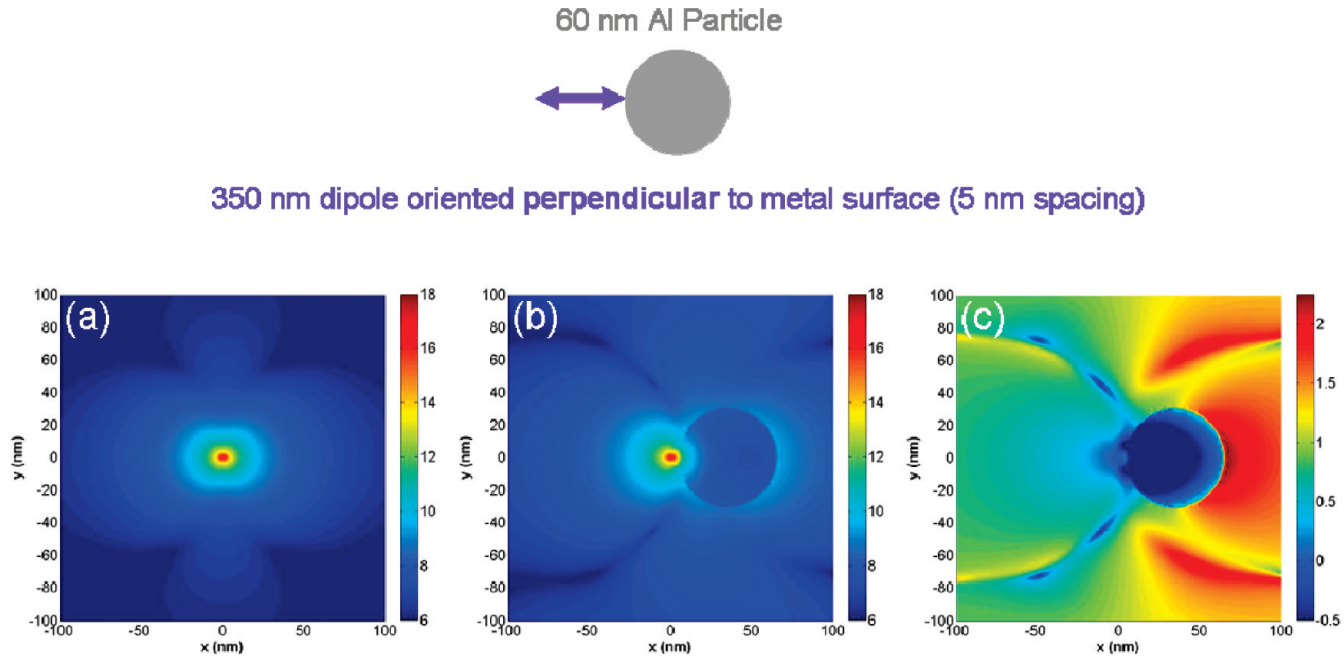

Figure 6. Near-field intensity distribution around (a) isolated perpendicular oriented dipole (along x axis) in water emitting at 350 nm, (b) a d = 60 nm aluminum nanoparticle with the dipole located at s = 5 nm from its surface calculated using FDTD, and (c) near-field enhancement and quenching. This image is generated by dividing the raw data of panel b by that of panel a. Note all images are displayed in the log scale.

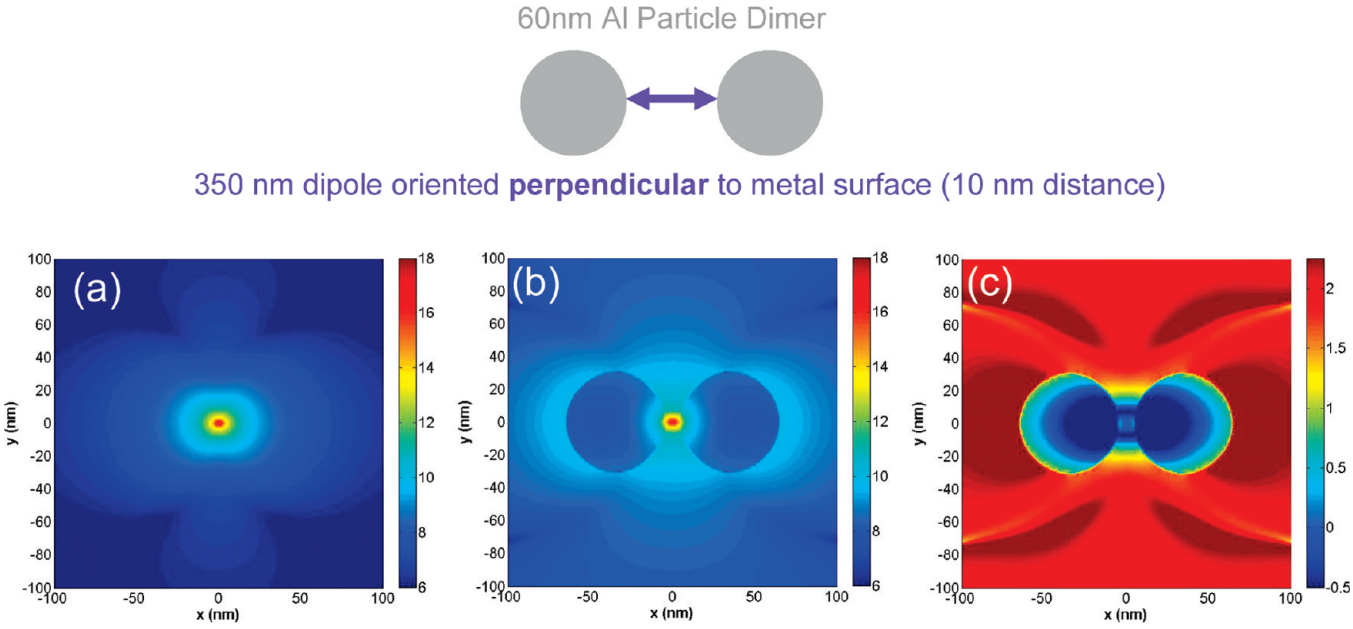

Figure 7. Near-field intensity distribution (in water) around (a) isolated perpendicular oriented dipole (along x axis) emitting at 350 nm, (b) a d = 60 nm aluminum nanoparticle dimer spaced $2s$ = 10 nm apart (surface−surface) with the dipole located in the middle calculated using FDTD, and (c) near-field enhancement and quenching. This image is generated by dividing the raw data of panel b by that of panel a. Note all images are displayed in the log scale.

that a nearby 350 nm dipole induces large near-fields around a d = 60 nm aluminum nanoparticle, and that these fields extend over tens of nanometers from the metal surface. We believe these fields contribute to the enhanced far-field radiation seen in Figure 3. The induced fields are even larger for a 350 nm dipole between two aluminum particles. Figure 7a−c shows respectively the electric field intensity in the x−y plane ($E^2 = E_x^2 + E_y^2 + E_z^2$) around an isolated fluorophore radiating at 350 nm, the near-fields around a d = 60 nm aluminum nanoparticle dimer system with a surface-to-surface distance of $2s$ = 10 nm and a perpendicularly oriented dipole located halfway between the particles, and the near-field enhancement and quenching image that was calculated by dividing the raw data of Figure 7b by the data of Figure 7a. In Figure 7c we see that the near-field is not enhanced in the gap between the particles, but there are intense field enhancements around all other areas of the particles. The intense near-field enhancement also extends tens of nanometers from the edge of the particles into the free space as observed by the extent of the red areas in the image. It is clear that the near-field enhancements of Figure 7c are much greater than those of the single aluminum nanoparticle [Figure 6c]. It is important to note that the near fields calculated in Figures 6 and 7 do not necessarily

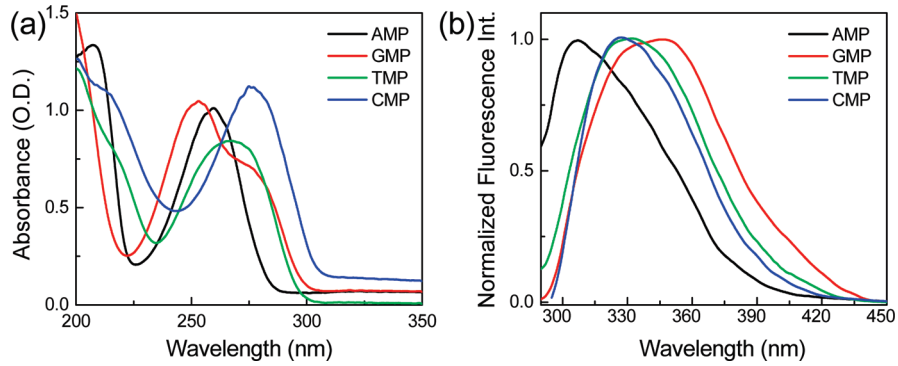

Figure 8. (a) Absorption spectra of DNA nucleotides in water and (b) emission spectra of DNA nucleotides in water.

represent propagating radiation. They could either be propagating fields or localized evanescent fields that are nonpropagating. In Figure 7c, only a small area between the two aluminum nanoparticles shows quenching. The overwhelmingly large portion of the image depicts significant near-field enhancements in the region immediately surrounding the dimer. We believe these near-field enhancements can potentially lead to enhancements in the far-field propagating emission (radiation) as shown in Figure 3. A comparison of the near-field distributions around an isolated fluorophore [Figure 7a] and a fluorophore in between two aluminum particles [Figure 7b] suggests a possible mechanism for MEF. Since the intensity of the excited-state fluorophore is actually decreased when it is in between the aluminum nanoparticles [Figure 7c], it suggests that the fluorophore alone is not the entity that is responsible for the enhanced emission. Rather it is the fluorophore coupled with the nearby aluminum nanoparticles that behaves together as a single radiating entity, which appears as the source of the enhanced fluorescence signals. We have coined the term "plasmaphore" to represent this coupled excited state dipole-metal radiating entity.[8]

We also performed experiments to corroborate the theoretical predictions above concerning the efficiency of aluminum nanostructures to detect unlabeled nucleotides using their intrinsic emission. Panels a and b in Figure 8 respectively show the absorption and emission spectra of the DNA nucleotides in water. The absorption spectra of the four bases are distinct. The emission from AMP and GMP are distinct, and the emission spectra of TMP and CMP are similar. In total these absorption and emission spectra show that the four bases could be identified using a combination of selected excitation and emission wavelengths if it is possible to detect an adequate number of photons above the background emission. As discussed in the Experimental Section, we spin-coated a 15 nm layer of polyvinyl alcohol (PVA) containing separately the dissolved DNA nucleotides CMP, GMP and TMP on a thin film of aluminum on a quartz slide and compared its emission intensity with an identical sample on a quartz substrate only (control). We have shown previously that such aluminum films are rough or nanostructured and so one might expect to see MEF similar to that predicted for the small nanoparticle limit here.[10]

Figure 9a shows a schematic of the sample geometry used in our experiments which consists of a 10 nm thick aluminum film vapor deposited on quartz slides. A 5 nm of silica was then evaporated on top of the aluminum film without breaking vacuum which serves to protect the metal surface as well as adds a spacer layer between the metal surface and DNA bases. Finally an approximately 15 nm thick layer of PVA containing separately dissolved GMP, CMP, and TMP was spin coated on the surface of the silica layers for the aluminum samples and directly on the quartz substrates for the control samples. Figure 9b shows that for a 15-nm thick polyvinyl alcohol (PVA) film containing thymidine 5′-monophosphate disodium salt hydrate (TMP), the 10 nm thick aluminum substrate gives an emission intensity enhancement of approximately 4-fold when compared to the quartz control. Figure 9c shows the fluorescence emission spectra of cytidine 5′-monophosphate (CMP) on top of a quartz and an aluminum substrate respectively, and we observe an approximately 5-fold increase in the emission intensity of the CMP on aluminum. Figure 9d shows the fluorescence emission spectra of guanosine 3′,5′-cyclic monophosphate sodium salt (GMP) on top of a quartz and the aluminum substrate respectively, where we observe an approximately 11-fold increase in the emission intensity of the GMP on aluminum. At present we have not yet obtained enhancements larger than 2-fold for AMP. The MEF is due to a through space interaction, and not dependent on chemical structure, and we are hopeful that greater enhanced AMP emission will also be observed in the near future. It is important to note that the enhanced fluorescence observed from the nucleotides on the 10 nm thick aluminum films cannot be attributed simply to conventional far-field reflection. Reflection occurs when the "metal substrate" is extended over several wavelengths in size. In the present case, the thermally evaporated aluminum particles are smaller than the wavelength of the excitation and emission,[9,10] so the 10 nm thick aluminum films essentially behave like a particulate surface. Additionally we would like to point out that since the PVA thickness is only 15 nm, all the nucleotides are approximately within 5−20 nm away from the metal surface (considering the 5 nm silica spacer layer), which is essentially in the near-field of metal particles. In this configuration we believe that the excited-state molecule couples to the plasmons on the surface of the aluminum particles and the combined excited fluorophore-metal complex acts as a unified system, which then radiates the emission observed in the experiments. The experimental results of Figure 9 corroborate the validity of our theoretical predictions that aluminum nanoparticles can be used to efficiently enhance the intrinsic emission of various DNA bases (in the UV region), and so creating the possibility of DNA sequencing based on the intrinsic base fluorescence, thus potentially avoiding the pitfalls involved in additional external labeling steps that are currently involved in DNA sequencing reactions.

We now consider how the increases in radiative rate will affect the quantum yields of the nucleotides near the metal

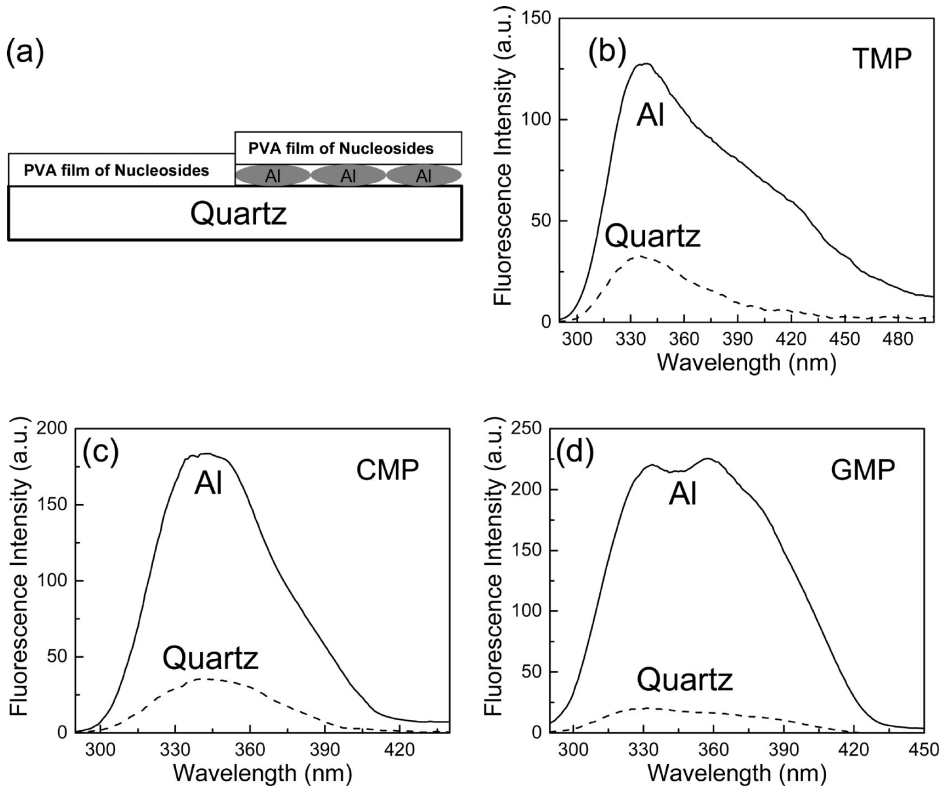

Figure 9. (a) Schematic of the sample geometry. Fluorescence spectra of a 15 nm thick PVA film on top of a 10 nm thick aluminum film, and on a quartz control that contain the DNA nucleotides (b) TMP, (c) CMP, and (d) GMP.

particle. The normal lifetime (τ_0) and quantum yield (Q_0) of a fluorophore in the absence of metal is given by[4,6]

$$Q_0 = \Gamma/(\Gamma + k_{nr}) \tag{3}$$

$$\tau_0 = (\Gamma + k_{nr})^{-1} \tag{4}$$

where Γand k_{nr} are the radiative and nonradiative decay rates respectively in the absence of metal. In the presence of metal nanostructures the new lifetime (τ_m) and quantum yield (Q_m) of the fluorophore becomes[4,6]

$$Q_m = \frac{\Gamma + \Gamma_m}{\Gamma + \Gamma_m + k_{nr}} \tag{5}$$

$$\tau_m = (\Gamma + \Gamma_m + k_{nr})^{-1} \tag{6}$$

where Γ_m is the radiative decay rate introduced in the presence of the metal. It is assumed that the metal does not modify the nonradiative decay rates. In the absence of metal, the typical lifetime of a DNA base is (τ_0) is 1 ps and the quantum yield is 2×10^{-4}.[46,47] Larger quantum yields have been reported but we selected a lower value to model a worst-case situation. Using eqs 3 and 4, these values correspond to $\Gamma = 2 \times 10^8$ s^{-1} and $k_{nr} = 1 \times 10^{12}$ s^{-1}. The starting quantum yield is low for DNA bases because the nonradiative decay k_{nr} is 5000-fold larger than the radiative rate Γ. The effect of the metal changes the radiative rate of the fluorophore to $\Gamma + \Gamma_m$, which results in the unique phenomenon of an increase in the quantum yield with a decrease in the lifetime as shown in Figure 10. The FDTD calculations of Figure 3 suggest that the radiative decay rates of DNA bases

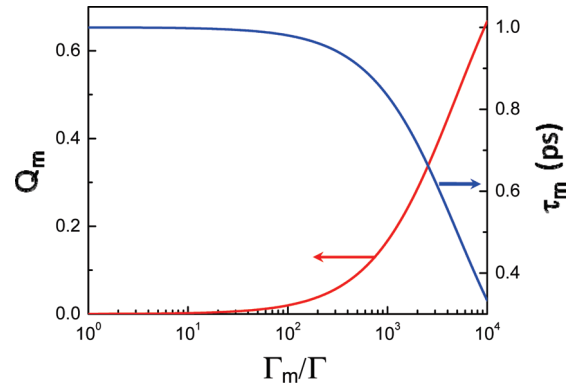

Figure 10. Effect of increase in the metal-induced radiative decay rates (Γ_m/Γ) on the quantum yield (Q_m) and lifetime (τ_m) of a typical DNA base.

can potentially be increased over 1000-fold when it is between two aluminum particles of appropriate size and shape, hence bringing the quantum yield of a DNA base near the metal (τ_m) up to 0.2, which is in range of the quantum yield of the Cy5 dye. It can be expected that proper design of metal nanoparticle-fluorophore systems can lead to even greater enhancements (increases in radiative decay rates) which would raise the quantum yield even higher. These considerations imply that obtainable increases in the rates of radiative decay can potentially result in DNA base quantum yields which are comparable to those of fluorophores routinely used in single molecule detection today (in the visible range).

In addition to increases in brightness the decreased lifetimes near metal particles are expected to make the bases more resistant to photobleaching. Fluorophores commonly used for single molecule detection have photobleaching quantum yields ranging from 10^{-5} to 10^{-6},[48,49] so that the fluorophore emits over 100 000 photons prior to photobleaching. The high

TABLE 1: Base Calling Accuracy Percentage (BCA%) of the Monte Carlo Simulation for Predicting DNA Nucleotides with One Excitation and Three Emission Wavelengths[a]

excitation (nm)	emission (nm)	# of photons	BCA% (A)	BCA% (G)	BCA% (T)	BCA% (C)
270	300, 330, and 360	500	99.25	62.63	98.86	66.46
270	300, 330, and 360	750	100.00	90.36	100.00	90.20
270	300, 330, and 360	1000	100.00	97.31	100.00	97.15
270	300, 330, and 360	1500	100.00	99.73	100.00	99.72
270	300, 330, and 360	2000	100.00	99.96	100.00	99.98
270	300, 330, and 360	2500	100.00	100.00	100.00	99.99
270	300, 330, and 360	5000	100.00	100.00	100.00	100.00
270	300, 330, and 360	10 000	100.00	100.00	100.00	100.00

[a] Dark current = 100 per channel and number of Monte Carlo cycles = 10 000 for all simulations.

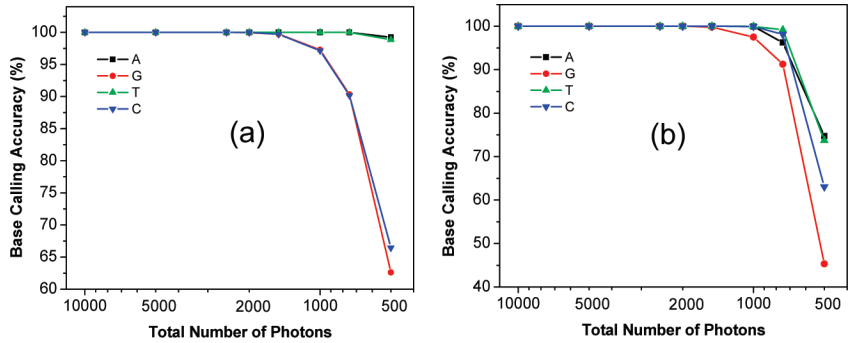

Figure 11. Base calling accuracy (%) as a function of total number of photons for Monte Carlo simulations involving: (a) One excitation (270 nm) and three emission (300, 330, and 360 nm) wavelengths. (b) Two excitation (260 and 280 nm) and two emission (305 and 350 nm) wavelengths.

nonradiative decay rate of the bases is expected to increase their photostability, as compared to typical fluorophores, because of the short time the bases remain in the excited state. Photodestruction occurs while the molecules are in the excited state. A further decrease in the decay times due to the effect of the metal is expected to decrease the photobleaching quantum yield and increase the number of emitted photons prior to photobleaching. Below we will show that it should be possible to detect and identify the bases with less than 2000 total detected photons with an accuracy of over 99.5%. Hence we expect the bases to display adequate photostability for sequencing. Additionally, we expect a reduction in the blinking because there is less time for transition to the triplet state or other dark states.

For DNA sequencing it is necessary to both detect and identify the bases. We believe it is possible to identify the bases because each base displays different absorption and emission spectra as shown in Figure 8. Although the spectral differences between the bases are not very large, we believe that the existing differences are enough to allow the bases to be identified using wavelength intensity ratio measurements at several wavelengths using a multiwavelength or array detector. We have used Monte Carlo simulations to predict the accuracy of base calling for an assumed number of photons. The Monte Carlo simulations were performed as follows. The assumed total number of photons were divided up among the emission channels. We then added an average of 100 photons of background to each emission channel. Poisson noise was added randomly to each intensity value. For each base, we performed 10 000 simulations and analyzed the results as described in the experimental section. We considered the use of one or two excitation wavelengths and two or three emission wavelengths. We varied the assumed number of photons to obtain a base calling accuracy of 99% or higher. Remarkably, less than 2000 photons are required to identify the bases with an accuracy of over 99.5%. In all of our Monte Carlo simulations, the dark current was limited to 100 counts per channel and the total number of Monte Carlo cycles was 10 000. Table 1 and Figure 11a shows the results for using one excitation (270 nm) and three emission (300, 330, and 360 nm) wavelengths. Here we see that by the time the total number of photons reaches 2,000, the base calling accuracy (BCA) of all the four DNA bases exceeds 99.9% - which is a remarkable result given the similarity of their spectral properties. Even better results are obtained for the case of two excitation (260 and 280 nm) and two emission (305 and 350 nm) wavelengths as shown in Table 2 and Figure 11b. Here we reach a BCA of greater than 99.9% by the time the total number of photons reaches only 1,500. These results indicate that an important contribution to base calling is the use of two excitation sources. However the results from the use of a single excitation source was very close to that of the two excitation source case. From an experimental standpoint, it is preferable to use a single excitation source from both a cost perspective, and the relative ease of setting up experiments in the UV.

Since DNA bases are known to have very low quantum yields (in the 10^{-5} to 10^{-4} range),[46] we believe enhancing the excitation and emission rates of intrinsic DNA base fluorescence alone might not be sufficient to have the appropriate signal intensity levels for accurate detection. It has been shown that plasmonic nanostructures with the correct dimensions can interact with light and lead to highly directional beaming effects.[50−54] This phenomenon is due to the electromagnetic surface resonances that is modulated by the dielectric properties of the metal. Given the fact that most experimental setups have a maximum signal collection efficiency of approximatley 5%, we believe it will be important to harness the beaming characteristics of the plasmonic nanostructures to increase the signal collection efficiency of the emission of the low quantum yield nucleotide fluorescence. We believe it will be possible to potentially design metallic nanostructures based on a central nanopore surrounded by corrugations as platforms for DNA sequencing and single nucleotide identification. We hope that this design will allow the added advantage of using the metallic nanostructures to lend

TABLE 2: Base Calling Accuracy Percentage (BCA%) of the Monte Carlo Simulation for Predicting DNA Nucleotides with Two Excitation and Two Emission Wavelengths[a]

excitation (nm)	emission (nm)	# of photons	BCA% (A)	BCA% (G)	BCA% (T)	BCA% (C)
260 and 280	305 and 350	500	74.71	45.32	73.71	63.05
260 and 280	305 and 350	750	96.23	91.26	99.15	98.13
260 and 280	305 and 350	1,000	99.95	97.52	99.96	99.93
260 and 280	305 and 350	1,500	100.00	99.98	100.00	100.00
260 and 280	305 and 350	2,000	100.00	100.00	100.00	100.00
260 and 280	305 and 350	2,500	100.00	100.00	100.00	99.99
260 and 280	305 and 350	5,000	100.00	100.00	100.00	100.00
260 and 280	305 and 350	10,000	100.00	100.00	100.00	100.00

[a] Dark current = 100 per channel and number of Monte Carlo cycles = 10 000 for all simulations.

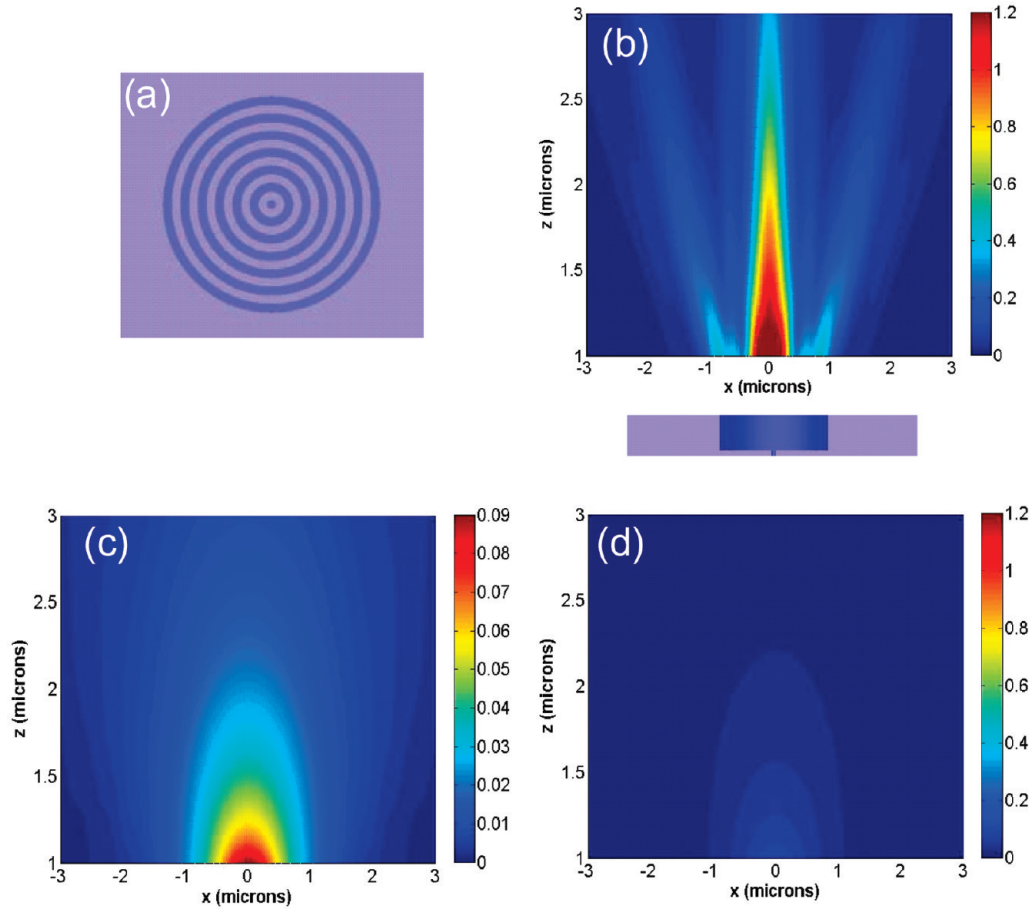

Figure 12. (a) Top view schematic of the aluminum nanostructure; (b) 350 nm dipole located in the middle of the central nanohole and polarized along the *x* axis, showing highly directional emission. The nanostructure dimensions were: nanohole diameter = 200 nm; thickness of aluminum film = 300 nm; no. of grooves around central nanohole = 6; groove thickness = 200 nm; groove depth = 250 nm; groove pitch = 400 nm (center−center). (c) Emission of 350 nm dipole in water. (d) Emission of 350 nm dipole in water with color scale matched to that of the dipole inside the aluminum nanostructure.

directionality to the otherwise isotropic emission from a fluorophore, thereby increasing its collection efficiency. To this end, we have performed some preliminary FDTD calculations that show a DNA base emitting at 350 nm inside an aluminum nanostructure that is composed of a central nanohole surrounded by a ring of corrugations can lead to highly directional emission. These results are presented in Figure 12. Figure 12a is a top view of the aluminum nanostructure used in the beaming calculations. The dimensions of the aluminum nanostructure are as follows: central nanohole diameter = 200 nm; thickness of the aluminum film = 300 nm; number of grooves around central nanohole = 6; groove thickness = 200 nm; groove depth = 250 nm; groove pitch = 400 nm (center−center). In all these calculations, the dipole was oriented along the *x*-axis, and was located in the middle of the central nanohole. Figure 12b shows for a dipole radiating at 350 nm, the emission is highly directional as it exits the aluminum nanostructure. Figure 12 (c) and (d) shows the emission of an identical dipole radiating at 350 nm in a homogeneous dielectric (which in our case is water) with no metallic nanostructures present. A close comparison of panel b with panels c and d in Figure 12 reveals two important observations: The interaction of the dipole with the aluminum nanostructure leads to a significant increase in the intensity of the emission from the fluorophore as observed in Figure 12, panels b and d, where both the colorbars are set to the same scale. This phenomenon is probably related to the extraordinary transmission of light that has been reported experimentally and predicted theoretically in recent years.[50,53,55] This intriguing effect is thought to be caused by the interaction of light (either dipoles or plane waves) with electronic reso-

nances in the surface of the corrugated metal film, and they can be controlled by adjusting the size and geometry of the features in the metallic nanostructure.[50,53,55] Figure 12c is the emission from the dipole in water, but the colormap has been scaled down to show clearly the emission pattern. Here we see a typical dipolar emission pattern distributed in half-space. When Figure 12c is compared with Figure 12b, it is obvious that the interaction of the dipole with the aluminum nanostructure leads to highly directional emission. Hence Figure 12b−d shows encouraging results that such aluminum nanostructures can not only increase the emission intensity of a DNA base located inside it, but also can lead to highly directional emission which can potentially increase the overall signal collection efficiency. We recognize that our calculations and conclusions are preliminary in nature and is meant to explore the possibility of using such structures to increase light collection efficiency.

4. Conclusions

In this paper, we present computational and experimental studies showing the possibility of using aluminum nanostructures for enhancing the intrinsic emission of the low quantum yield DNA nucleotides in the ultraviolet region, thus suggesting that such metallic nanostructures hold potential in the future for designing high-throughput, low-cost DNA sequencing studies using the intrinsic fluorescence of DNA bases. In our FDTD calculations, the excited fluorophore was modeled as a oscillating dipole source, and a variety of spherical nanoparticle sizes, and fluorophore-nanoparticle distances relative to the aluminum surface were studied.

We observed that computing the wavelength-dependent radiated power enhancement spectra of aluminum for a range of nanoparticle sizes shows consistent enhancements in the 300−350 nm range which is relevant for intrinsic nucleotide fluorescence. The peak enhancement wavelength is a function of the nanoparticle size, with larger nanoparticles showing enhancement peaks at longer wavelengths. Additionally, the degree of enhancement of the radiated power increased significantly when the fluorophore is placed in between two aluminum nanoparticles of a dimer system. In the nanoparticle systems investigated in this study, we observe maximum enhancements of over 800-fold when the fluorophore is located between two $d = 60$ nm aluminum nanoparticles spaced $2s = 4$ nm apart (surface−surface). We purposely performed our radiative power FDTD calculations with the dipole oriented perpendicular to the metal surface as we know that this orientation is expected to give the maximum enhancements (as opposed to the dipole oriented parallel to the metal surface).[10,32]

We investigated the effect of the excitation light (plane waves) as well as excited-state fluorophores on the near-fields around the metal nanoparticles. Inspection of near-field intensity patterns revealed that very specific regions around the nanoparticles experience field enhancements. These kind of results are not easily inferred from radiatve power and other far-field calculations and can be of potential interest in spatially resolved molecular spectroscopy or detection using fluorescence.

We also present experimental results showing that thin aluminum films when compared to quartz substrates can significantly enhance the emission intensity of a layer of polyvinyl alcohol (PVA) film containing separately the dissolved DNA nucleotides GMP, TMP, and CMP. These observations corroborate our theoretical predictions that aluminum nanoparticles are efficient substrates for enhancing the intrinsic fluorescence of the low quantum yield DNA nucleotides that emit in the UV.

We present Monte Carlo simulations to predict the accuracy of base calling for an assumed number of photons. The algorithm identifies the different bases using wavelength intensity ratio measurements at several wavelengths. Our results show that a total number of photon count of less 2000 are required to identify the four bases with an accuracy of over 99.5%. Our results also indicate that an important contribution to base calling is the use of two excitation sources, although the results from the use of a single excitation source were close enough to the two excitation source case. Hence we predict that using a single excitation source might be more convenient due to the ease of experimental setup and design.

Finally we also present some preliminary FDTD calculations that show a dipole radiating at 350 nm when coupled to a patterned aluminum nanostructure containing a central nanohole can lead to enhanced and highly directional emission when compared to an isolated dipole in a dielectric. These set of calculations indicate that such structures can potentially be used in nanopore based DNA sequencing studies which can help in significantly increasing the collection efficiency of the emission of the bases. This will be of particular importance for the intrinsic emission of bases because DNA bases have very low quantum yields.

We would like to reiterate that we are acutely aware of the fact that the DNA nucleotides have very low quantum yields and thus are cognizant of the numerous obstacles that can appear in designing an intrinsic nucleotide fluorescence based DNA sequencing system. The goal of this study is only to investigate the possibility of using aluminum nanostructures for enhancing the intrinsic base fluorescence of DNA bases and also increasing its collection efficiency. This is only the first step in a study that we hope will ignite interest in the broader scientific community to take advantage of the plasmonic properties of aluminum and the potential benefits of its interaction with DNA bases. We hope this study will generate momentum toward accomplishing the goal of designing low-cost high-throughput DNA sequencing devices using the intrinsic fluorescence of bases.

Acknowledgment. This work was supported by the National Institutes of Health - NHGRI (Grant Nos. HG005090 and HG002655), and NIBIB (Grant no. EB006521). M.L.J. was supported by the National Institutes of Health - NCRR (grant No. RR019991). Use of the Center for Nanoscale Materials was supported by the U.S. Department of Energy, Office of Science, Office of Basic Energy Sciences, under Contract No. DE-AC02-06CH11357.

References and Notes

(1) Weber, G. *Biochem. J.* **1960**, *75*, 335.
(2) Konev, S. V. *Fluorescence and phosphorescence of proteins and nucleic acids*; Plenum Press: New York, 1967.
(3) Demchenko, A. P. *Ultraviolet spectroscopy of proteins*; Springer-Verlag: New York, 1981.
(4) Lakowicz, J. R. *Principles of Fluorescence Spectroscopy*, 3rd ed.; Springer: New York, 2006.
(5) Zhang, J.; Fu, Y.; Chowdhury, M. H.; Lakowicz, J. R. *Nano Lett.* **2007**, *7*, 2101–2107.
(6) Lakowicz, J. R. *Anal. Biochem.* **2001**, *298*, 1–24.
(7) Lakowicz, J. R. *Anal. Biochem.* **2005**, *337*, 171–194.
(8) Lakowicz, J. R.; Ray, K.; Chowdhury, M.; Szmacinski, H.; Fu, Y.; Zhang, J.; Nowaczyk, K. *The Analyst* **2008**, *133*, 1308–1346.
(9) Ray, K.; Chowdhury, M. H.; Lakowicz, J. R. *Anal. Chem.* **2007**, *79*, 6480.
(10) Chowdhury, M. H.; Ray, K.; Gray, S. K.; Pond, J.; Lakowicz, J. R. *Anal. Chem.* **2009**, *81*, 1397.
(11) Ray, K.; Szmacinski, H.; Lakowicz, J. R. *Anal. Chem.* **2009**, *81*, 6049.
(12) Metzker, M. L. *Genome Res.* **2005**, *15*, 1767.

(13) Shendure, J.; Mitra, R. D.; Varma, C.; Church, G. M. *Nature Rev.* **2004**, *5*, 335.
(14) Zwolak, M.; DiVentra, M. *Rev. Mod. Phys.* **2008**, *80*, 141–165.
(15) Marziali, A.; Akeson, M. *Annu. Rev. Biomed. Engr.* **2001**, *3*, 195.
(16) VonBulnof, A. *Cell* **2008**, *132*, 721.
(17) International Human Genome Sequencing Consortium. *Nature* 2001, *409*, 860.
(18) Venter, J. C. *Science* **2001**, *291*, 1304.
(19) Sanger, F.; Nicklen, S.; Coulson, A. R. *Proc. Natl. Acad. Sci.* **1977**, *74*, 5463.
(20) Smith, L. M.; Sanders, J. Z.; Kaiser, R. J.; Hughes, P.; Dodd, C.; Connell, C. R.; Heiner, C.; Kent, S. B. H.; Hood, L. E. *Nature* **1986**, *321*, 674.
(21) Prober, J. M.; Trainor, G. L.; Dam, R. J.; Hobbs, F. W.; Robertson, C. W.; Zagursky, R. J.; Cocuzza, A. J.; Jensen, M. A.; Baumeister, K. *Science* **1987**, *238*, 336.
(22) Guo, J.; Xu, N.; Li, Z.; Zhang, S.; Wu, J.; Kim, D. H.; Marma, M. S.; Meng, Q.; Cao, H.; Li, X.; Shi, S.; Yu, L.; Kalachikov, S.; Russo, J. J.; Turro, N. J.; Ju, J. *Proc. Natl. Acad. Sci.* **2008**, *105* (27), 9145.
(23) Deamer, D. W.; Branton, D. *Acc. Chem. Res.* **2002**, *35* (10), 817.
(24) Bayley, H. *Current. Opin. Chem. Biol.* **2006**, *10*, 628.
(25) Astier, Y.; Braha, O.; Bayley, H. *J. Am. Chem. Soc.* **2006**, *128*, 1705.
(26) Pushkarev, D.; Neff, N. F.; Quake, S. R. *Nat. Biotechnol.* **2009**, *27* (9), 847.
(27) Eid, J.; et. al. *Science* **2009**, *323*, 133.
(28) Földes-Papp, Z.; Angerer, B.; Thyberg, P.; Hinz, M.; Wennmalm, S.; Ankenbauer, W.; Seliger, H.; Holmgren, A.; Rigler, R. *J. Biotechnol.* **2001**, *86*, 203.
(29) Stephan, J.; Dorre, K.; Brakmann, S.; Winkler, T.; Wetzel, T.; Lapczyna, M.; Stuke, M.; Angerer, B.; Ankenbauer, W.; Földes-Papp, Z.; Rigler, R.; Eigen, M. *J. Biotechnol.* **2001**, *86*, 225.
(30) Chan, E. Y. *Mutat. Res.* **2005**, *573*, 13.
(31) Chowdhury, M. H.; Gray, S. K.; Pond, J.; Geddes, C. D.; Aslan, K.; Lakowicz, J. R. *J. Opt. Soc. Am. B* **2007**, *24*, 2259.
(32) Chowdhury, M. H.; Pond, J.; Gray, S. K.; Lakowicz, J. R. *J. Phys. Chem. C* **2008**, *112*, 11236.
(33) Taflove, A.; Hagness, S. C. *Computational Electrodynamics: The Finite-Difference Time-Domain Method*, 3rd ed.; Artech House: Norwood, 2005.
(34) Sullivan, D. M. *Electromagnetic Simulation Using the FDTD Method*; IEEE Press: Piscataway, 2000.
(35) Taflove, A.; Brodwin, M. E. *IEEE Trans. Microwave Theory Tech.* **1975**, *23*, 623.
(36) Yee, K. S. IEEE Trans. Antennas Propagat. 1966, AP-14302.
(37) Guiffaunt, G.; Mahdjoubi, K. *IEEE Ant. And Prop. Mag.* **2001**, *43*, 94.
(38) Berenger, J. P. *J. Comput. Phys.* **1994**, *114*, 185.
(39) Kaminski, F.; Sandoghdar, V.; Agio, M. *J. Comp. and Theor. Nanoscience* **2007**, *4*, 635.
(40) Reference Guide for FDTD Solutions Release 5.0 (2007), http://www.lumerical.com/fdtd.
(41) Metropolis, N.; Ulam, S. *J. Am. Statis. Assoc.* **1949**, *44* (247), 335.
(42) Rubinstein, R. Y.; Kroese, D. P. *Simulation and the Monte Carlo Method*, 2nd ed.; John Wiley & Sons: New York, 2007.
(43) Robert, C. P.; Casella, G. *Monte Carlo Statistical Methods*, 2nd ed.; Springer: New York, 2005.
(44) Gryczynski, I.; Malicka, J.; Nowaczyk, K.; Gryczynski, Z.; Lakowicz, J. R. *J. Phys. Chem. B* **2004**, *108*, 12073.
(45) Ruppin, R. *J. Chem. Phys.* **1982**, *76*, 1681.
(46) Peon, J.; Zewail, A. H. *Chem. Phys. Lett.* **2001**, *348*, 255.
(47) Malone, R. J.; Miller, A. M.; Kohler, B. *Photochem. Photobiol.* **2003**, *77*, 158.
(48) Soper, S. A.; Nutter, H. L.; Keller, R. A.; Davis, L. M.; Shera, E. B. *Photochem. Photobiol.* **1993**, *57* (6), 972.
(49) Eggeling, C.; Widengren, J.; Rigler, R.; Seidel, C. A. M. Photostability of fluorescent dyes for single-molecule spectroscopy: mechanisms and experimental methods for estimating photobleaching in aqueous solution. In *Applied fluorescence in chemistry, biology and medicine*; Rettig, W., Strehmel, B., Schrader, S., Seifert, H., Eds.; Springer-Verlag: New York, 1999; p 193.
(50) Barnes, W. L.; Dereux, A.; Ebbesen, T. W. *Nature* **2003**, *424*, 824.
(51) Wang, B.; Wang, G. P. *Appl. Phys. Lett.* **2006**, *88*, 013114.
(52) Lin, D. Z.; Chang, C. K.; Chen, Y. C.; Yang, D. L.; Lin, M. W.; Yeh, J. T.; Liu, J. M.; Kuan, C. H.; Yeh, C. S.; Lee, C. K. *Opt. Expr.* **2006**, *14* (8), 3503.
(53) Genet, C.; Ebbesen, T. W. *Nature* **2007**, *445*, 39.
(54) Soni, G. V.; Meller, A. *Clin. Chem.* **2007**, *53* (11), 1.
(55) Chowdhury, M. H.; Catchmark, J. M.; Lakowicz, J. R. *Appl. Phys. Lett.* **2007**, *91*, 103118.

JP911229C